Numerical modeling of wind turbine aerodynamic noise in the time domain

Seunghoon Lee and Seungmin Lee

AeroAcoustics and Noise Control Laboratory, Department of Mechanical and Aerospace Engineering, Seoul National University, Seoul 151-744, Republic of Korea
kami00@snu.ac.kr, vitamin1@snu.ac.kr

Soogab Lee[a]

Center for Environmental Noise and Vibration Research, Engineering Research Institute, Department of Mechanical and Aerospace Engineering, Seoul National University, Seoul 151-744, Republic of Korea
solee@snu.ac.kr

Abstract: Aerodynamic noise from a wind turbine is numerically modeled in the time domain. An analytic trailing edge noise model is used to determine the unsteady pressure on the blade surface. The far-field noise due to the unsteady pressure is calculated using the acoustic analogy theory. By using a strip theory approach, the two-dimensional noise model is applied to rotating wind turbine blades. The numerical results indicate that, although the operating and atmospheric conditions are identical, the acoustical characteristics of wind turbine noise can be quite different with respect to the distance and direction from the wind turbine.
© 2013 Acoustical Society of America

1. Introduction

Although aerodynamic noise from modern wind turbines is low compared to other community noise sources, wind turbine noise can annoy residents near wind farms.[1–3] One of the reasons for this annoyance is that wind turbines generate a periodic swishing sound at the blade passing frequency.[2] This is known as the amplitude modulation of wind turbine noise. In the vicinity of a wind turbine, this swishing sound is heard due to convective amplification and trailing edge noise directivity.[4] However, van den Berg[3] reported that sometimes at night, a periodic thumping sound was perceived at distances of more than 1 km from wind turbines and that this thumping sound had a more impulsive characteristic compared to the swishing sound. He maintained that a stable atmospheric condition at night is the main cause of the thumping sound. Oerlemans and Schepers[5] calculated the swish amplitude of wind turbine noise using a semi-empirical model.[6] They claimed that in the crosswind direction, wind turbine noise retains the amplitude modulation even at long distances. However, it is still not known why the perceived sounds are different and how they differ depending on observer locations.

In this study, to compare the acoustical characteristics of wind turbine noise depending on the observer location, the aerodynamic noise from a wind turbine is numerically modeled in the time domain. Because the time domain simulation directly provides the acoustic pressure of the wind turbine noise, we can actually hear the predicted acoustic signals. This helps us to better understand the acoustical characteristics of the wind turbine noise with respect to the distance and direction from the wind turbine. In Sec. 2, a numerical procedure for the modeling of wind turbine noise is described. Section 3 presents the calculated acoustic signals and their sound pressure

---

[a]Author to whom correspondence should be addressed.

levels at a number of locations. Using these results, the characteristics of the amplitude modulation of wind turbine noise are discussed in Sec. 4.

2. Method

2.1 Trailing edge noise model

The model proposed by Amiet[7,8] is used for the modeling of the trailing edge noise, which is known to be the main source of wind turbine aerodynamic noise.[4] This model assumes that the airfoil is a flat plate in rectilinear motion and provides the chordwise surface pressure distribution of the flat plate.

A rectangular flat plate is placed on the plane $x_3 = 0$, and it moves with velocity U in the negative x_1 direction. The trailing edge of the plate is aligned with the x_2 axis, and the origin of the Cartesian coordinate system is at the center of the trailing edge. The surface pressure jump at point **y** at time t can then be described as

$$\Delta p(y_1, y_2, t) = \iint_{-\infty}^{\infty} p_0(k_c, k_2) e^{-i\{k_c(y_1 - U_c t) + k_2 y_2\}} \{e^{\varepsilon k_c y_1} - 1$$
$$+ (1 + i)E^*[-y_1(k_c + \mu M + \zeta)]\} dk_c dk_2, \tag{1}$$

where p_0 is the amplitude of the pressure wavenumber component, k_c is the streamwise convective wavenumber, k_2 is the spanwise wavenumber, U_c is the convection velocity, M is the Mach number, $\mu = Mk_c U_c / \beta^2 U$, $\beta = \sqrt{1 - M^2}$, and $\zeta = \sqrt{\mu^2 - k_2^2 / \beta^2}$. Here $E^*[\ ]$ represents the complex conjugate of the Fresnel integral. The exponential convergence factor $e^{\varepsilon k_c y_1}$ is introduced to reduce the abrupt increase in the surface pressure at the leading edge.[8]

In order to simplify the integration in Eq. (1), the surface pressure is assumed to be independent of the spanwise wavenumber, i.e., $k_2 = 0$.[9] Moreover, the convection velocity is assumed to be constant, and it is set to $U_c = 0.6U$. Thus, Eq. (1) becomes

$$\Delta p(y_1, t) = \int_{-\infty}^{\infty} p_0 e^{-ik_c(y_1 - U_c t)} \{e^{\varepsilon k_c y_1} - 1 + (1 + i)E^*[-y_1\{k_c + \mu(1 + M)\}]\} dk_c. \tag{2}$$

Equation (2) is numerically integrated by the method described in earlier work.[10] This is given by

$$\Delta p(y_1, t) \approx -4\pi \sum_{n=1}^{N} A_n e^{-i\{k_{c,n}(y_1 - U_c t) + \psi_n\}} \{e^{\varepsilon k_{c,n} y_1} - 1 + (1 + i)E^*[-y_1\{k_{c,n} + \mu(1 + M)\}]\}, \tag{3}$$

where $A_n = \sqrt{\Phi_{qq}(k_{c,n}, 0, k_c U_c)\Delta k_c}$, ψ_n are independent random variables uniformly distributed at $[0, 2\pi]$, $\Phi_{qq}(k_c, k_2, \omega)$ is the wall-pressure wavenumber-frequency spectrum, $k_{c,n}$ are the streamwise convective wavenumbers, and N is the number of computing wavenumbers.[10] Hence, the real value of Eq. (3) is the fluctuating pressure on the surface, and this is used as the input for the calculation of the far-field acoustic pressure.

The wall-pressure wavenumber-frequency spectrum is the Fourier wavenumber spectrum of the incident pressure field on the surface. This spectrum can be empirically modeled as the following equation provided that the convection velocity is constant:

$$\Phi_{qq}(\omega/U_c, 0, \omega) = (U_c/\pi)S_{pp}(\omega)l_2(\omega). \tag{4}$$

In Eq. (4), $S_{pp}(\omega)$ is the wall point pressure frequency spectrum, and $l_2(\omega)$ is the turbulence correlation length in the spanwise direction.[9] In principle, the wall point pressure spectrum can be accurately obtained by wind tunnel experiments or large eddy simulations. It can also be determined by Reynolds-averaged Navier-Stokes simulations

with an appropriate empirical model.[11] However, the purpose of this study is to evaluate the acoustical characteristics of wind turbine noise, rather than find an exact prediction of the acoustic frequency spectrum. Accordingly, a simple empirical formula proposed by Kim and George[12] is used, which is given by

$$S_{pp}(\omega) = (\rho_0 U^2/2)^2 (\delta^*/U) S_0(\tilde{\omega}), \tag{5}$$

where $\tilde{\omega} = \omega \delta^*/U$ and δ^* is the boundary layer displacement thickness. Here $S_0(\tilde{\omega})$ is approximated by

$$S_0(\tilde{\omega}) = (1.732 \times 10^{-3}\tilde{\omega})/(1 - 5.489\tilde{\omega} + 36.74\tilde{\omega}^2 + 0.1505\tilde{\omega}^5), \tag{6}$$

for $\tilde{\omega} < 0.06$, and

$$S_0(\tilde{\omega}) = \frac{1.4216 \times 10^{-3}\tilde{\omega}}{0.3261 + 4.1837\tilde{\omega} + 22.818\tilde{\omega}^2 + 0.0013\tilde{\omega}^3 + 0.0028\tilde{\omega}^5}, \tag{7}$$

for $0.06 < \tilde{\omega} < 20$. In addition, the correlation length is determined from an experiment by Brooks and Hodgson.[13] This is given by

$$l_2(\omega) = U_c/0.6\omega. \tag{8}$$

2.2 Acoustic formulation

Formulation 1 A by Farassat[14] is used to calculate the far-field acoustic pressure radiating from wind turbine blades. Formulation 1 A is one of the integral forms of the Ffowcs Williams and Hawkings equation, which is well suited for numerical calculations. This formulation is composed of thickness and loading noise terms, but the thickness term is neglected in the present study. This is because the trailing edge noise mechanism when the flow is at a low Mach number is closely associated with the loading noise. With this formulation, the far-field acoustic pressure can be expressed as

$$4\pi p'(\mathbf{x}, t) = \frac{1}{c_0} \int \left[\frac{\dot{p}_i \hat{r}_i}{r(1 - M_r)^2} \right]_{\text{ret}} dS + \int \left[\frac{p_r - p_i M_i}{r^2(1 - M_r)^2} \right]_{\text{ret}} dS$$
$$+ \frac{1}{c_0} \int \left[\frac{p_r(r\dot{M}_i \hat{r}_i + c_0 M_r - c_0 M^2)}{r^2(1 - M_r)^3} \right]_{\text{ret}} dS, \tag{9}$$

where $\mathbf{x}$ and $\mathbf{y}$ are the observer and the source locations, respectively; $r = |\mathbf{x} - \mathbf{y}|$ is the radiation distance; dS is an element of surface area of blade; and $\hat{\mathbf{r}} = (\mathbf{x} - \mathbf{y})/|\mathbf{x} - \mathbf{y}|$ is the unit radiation vector. The subscript r indicates a component in the radiation direction, and the dots represent a derivative with respect to the source time. The square brackets $[\ ]_{\text{ret}}$ indicate that the integration is evaluated at a retarded time. The surface pressure vector $\mathbf{p}$ in Eq. (9) is the real value of $\Delta p(y_1, \tau)$ in Eq. (3) in the normal direction from the surface.

2.3 Validation

Validation for a two-dimensional (2D) flow is carried out via a comparison with the result of the experiment by Brooks *et al.*[6] The case of interest here is the tripped boundary layer case of the 2D sharp trailing edge model at a zero angle of attack. The inflow velocities used in the validation case are $U = 55.5$ and 71.3 m/s. For the numerical prediction of the trailing edge noise, the airfoil is modeled as a flat-plate grid which has the same span and chord length as the experiment model. The rectangular surface grid is clustered near the trailing edge, while it is uniformly applied in the spanwise

direction. The longest chordwise grid is sufficiently small to resolve the highest frequency. The maximum frequency for the acoustic prediction is set to $f_N = 10\,\text{kHz}$. The frequency range is divided into $N = 1000$ partitions for numerical integration. Consequently, the bandwidth and the minimum frequency become $f_1 = \Delta f = 10\,\text{Hz}$. The boundary layer thickness in Eq. (5) is calculated from the empirical formula proposed in an earlier study.[6] The calculation is performed during one period of the minimum frequency, i.e., $T = 0.1\,\text{s}$. Figure 1(a) compares the 1/3 octave band spectra between the experimental data and the numerical result. The sound pressure levels predicted by the numerical model agree well with those of the experimental data to within $\pm 3\,\text{dB}$.

This study also investigates the noise directivity of the model airfoil. The noise is calculated in the range from $\theta = 0°$ to $\theta = 360°$ in steps of $1°$. The narrowband spectra for each acoustic pressure are obtained by applying a fast Fourier transform to the acoustic signals. Each frequency component is then extracted at each observer location. The directivity is determined by the root-mean-square pressure of the narrowband spectrum. Figure 1(b) shows the streamwise noise directivity for the frequency bands at $100\,\text{Hz}$, $500\,\text{Hz}$, $1\,\text{kHz}$, and $5\,\text{kHz}$. Each curve is normalized by its maximum value. For low-frequency bands, the directivity appears to be similar to a dipole source. On the other hand, as the frequency increases, multiple lobes emerge and the directivity becomes similar to a cardioid pattern. This trend is identical to those observed in previous studies.

2.4 Rotor noise prediction

The wind turbine model used in the calculation is a 2.5 MW three-blade horizontal axis wind turbine that has typical multi-MW wind turbine characteristics. This turbine is a pitch regulated, variable speed type with a rotor diameter of 93 m and a hub height of 82 m. In this study, noise is predicted at a wind speed of 10 m/s, which is assumed to be uniform over the rotor plane.

A strip theory approach is used to apply the 2D noise model to the rotating blades. The blades are divided into 20 segments of equal lengths. Each segment is modeled as a flat-plate grid. Because the blade span is very large compared to the turbulence correlation length in the spanwise direction, it is assumed that the fluctuating surface pressure has no correlation between the segments. The inflow velocity and the effective angle of attack are assumed as uniform in each segment. They are calculated by an in-house program that uses the blade element momentum theory. The boundary layer displacement thickness, which is necessary for the prediction of the wall point pressure frequency spectrum, is obtained with the XFOIL code.[15]

The calculations are performed for a duration of one-third of a rotation, i.e., $T = 1/f_{\text{BPF}}$. The maximum frequency and the frequency bandwidth are set to $f_N = 5\,\text{kHz}$
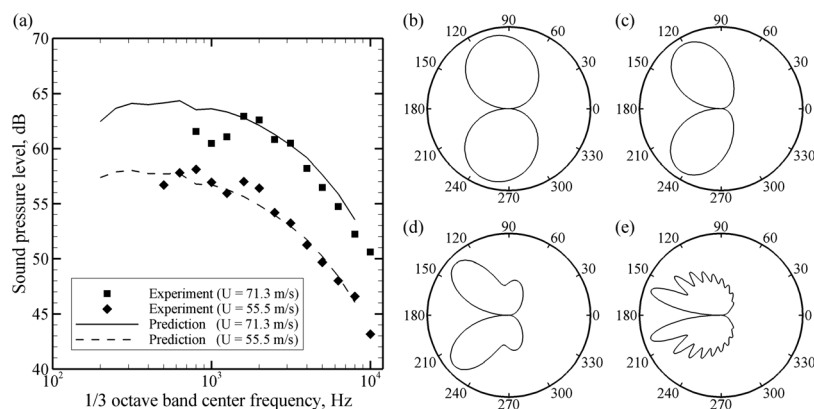
Fig. 1. (a) Comparison of the 1/3 octave band spectra between the numerical predictions and the results of the experiment by Brooks *et al.* (Ref. 6). (b) Streamwise noise directivity in the mid-span plane for frequencies of $f = 100\,\text{Hz}$, (c) $f = 500\,\text{Hz}$, (d) $f = 1\,\text{kHz}$, and (e) $f = 5\,\text{kHz}$.

and $\Delta f = 10\,\text{Hz}$, respectively. The time step is set to $\Delta T = 0.1\,\text{ms}$, which satisfies the Nyquist sampling criterion. Moreover, for the calculation of air absorption, it is assumed that the air temperature is $15\,^{\circ}\text{C}$, the relative humidity is 60%, and the air pressure is one standard atmosphere. The approximate attenuated sound levels are determined by the multiplication of the attenuation coefficients and the radiation distance in kilometers;[16] this is set as the distance between the center of the rotor hub and an observer location. The calculated acoustic signals are filtered by finite impulse response filters with an arbitrary magnitude to apply the attenuated sound levels. In addition, acoustic reflections from the ground and acoustic refraction caused by wind and temperature gradients are not considered in this calculation.

3. Results

The acoustic signals are calculated at distances of $R = 128.5$, 250, 500, and $1000\,\text{m}$ from the wind turbine at azimuthal intervals of 15°. The sound pressure level and the modulation depth of the predicted signals are presented in Fig. 2. The results show that the sound pressure level reaches its maximum in the upwind and downwind directions, while it reaches its minimum in the crosswind direction. On the other hand, the modulation depth is greatest in the crosswind direction, whereas it is small in the upwind and downwind directions.

The acoustical characteristics of the amplitude modulation in wind turbine noise are evaluated in terms of observer locations by comparing a part of the predicted signals presented at Mm. 1 and 2. In the vicinity of the wind turbine (Mm. 1), the amplitude modulation is detected from all azimuthal directions. These sounds are similar to a typical swishing sound. On the other hand, at long distances from the wind turbine (Mm. 2), the amplitude modulation is hardly perceived in the upwind, downwind, and crosswind directions; the amplitude modulation disappears in the upwind and downwind directions, and the noise level is too low to be heard in the crosswind direction. Nevertheless, even at long distances the amplitude modulation is still audible in other directions provided that the background noise is low. In addition, these sounds are no longer similar to the swishing sound. They are low-frequency amplitude-modulated sounds, as most of the high-frequency noise is attenuated due to air absorption.

Mm. 1. This audio is the sum of 13 acoustic signals, which are predicted at a distance of $R = 128.5\,\text{m}$ with an azimuth angle ranging from $\Psi = 0^{\circ}$ to $\Psi = 180^{\circ}$ at intervals of 15°. Each signal repeats three times, and there is an interval of 1 s between different signals. This is a file of type "wav" (1.2 MB).
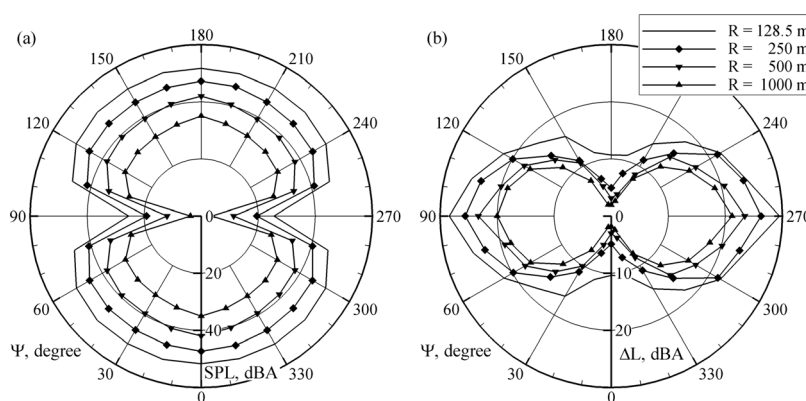
Fig. 2. (a) The A-weighted sound pressure level and (b) the modulation depth of the predicted acoustic signals. The azimuth angle Ψ is defined as the angle between the rotor axis and the line connecting the wind turbine to the observer. The wind is blowing from the $\Psi = 180^{\circ}$ direction. The modulation depth is defined as the difference between L_{AFmax} and L_{AFmin}.

Mm. 2. This audio is the sum of 13 acoustic signals, which are predicted at a distance of $R = 1000$ m with an azimuth angle ranging from $\Psi = 0°$ to $\Psi = 180°$ at intervals of $15°$. Each signal repeats three times, and there is an interval of 1 s between different signals. This is a file of type "wav" (1.2 MB).

Moreover, the noise source distribution on the rotor disk is calculated to examine how the amplitude modulation in wind turbine noise is generated depending on the observer location. The source distributions of different observer locations are compared in Fig. 3. The asymmetry of the source distribution along the azimuthal direction is clearly apparent. This asymmetry is the cause of the amplitude modulation. The black contours in the figures indicate the regions at which the swishing sound is generated. The locations and the shapes of these regions are dependent on the observer position. These regions correspond to the positions where the blades approach the observer.

The results indicate that the asymmetric shapes are different with respect to the distance and direction from the wind turbine. In the downwind direction ($\Psi = 0°$), the asymmetry of the source distribution along the azimuthal direction gradually disappears as the distance increases. On the other hand, the strength of this asymmetry remains the same in the $\Psi = \pm 60°$ directions, or it slowly decreases but does not disappear in the $\Psi = \pm 30°$ directions. Note that the locations on the rotor where the maximum sound levels are generated vary as the distance to the observer increases. In the direction where the blades pass downward ($0° < \Psi < 180°$), this location rises to the top of the rotor disk as the distance increases. On the other hand, in the direction where the blades pass upward ($180° < \Psi < 360°$), this location moves slightly toward the bottom of the rotor disk as the distance increases.

4. Discussion

The acoustical characteristics of wind turbine noise are quite different with respect to the distance and direction from the wind turbine, although the operating and atmospheric conditions are identical. In the vicinity of a wind turbine, typical swishing sounds are perceived from all azimuthal directions. On the other hand, at long distances from a wind turbine, low-frequency amplitude-modulated sounds are heard in particular directions. Moreover, in contrast to the swishing sounds, these low-frequency sounds are heard only at the moments when the sound pressure level is sufficiently high, e.g., when the blades pass the black contours shown in Fig. 3. This effect may
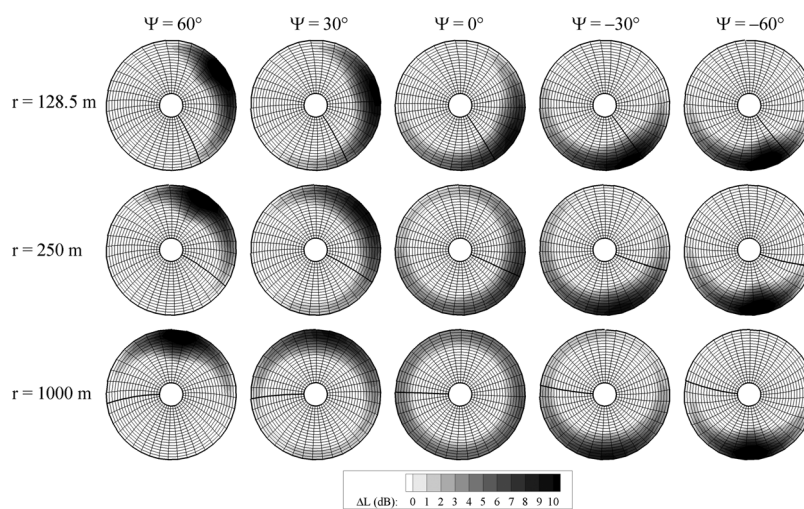
Fig. 3. Level difference between the calculated source distribution and the average sound pressure level of the rotor disk. The source distributions are calculated at three distances in five directions. For each source distribution, the average level of the total segment for the overall time is subtracted from the sound pressure level distribution on the rotor disk. This makes it possible to compare source distributions whose overall sound levels are different.

make the wind turbine noise seem more impulsive at long distances despite the fact that its overall sound pressure level is low.

van den Berg[3] suggested that the thumping sound occurs due to excessive vertical wind shear at night. However, the results from this study indicate that even when a uniform wind is blowing into the rotor disk, different types of noise can be heard depending on the observer location. This implies that the main cause of the thumping sound could be the convective amplification and the trailing edge noise directivity rather than the strong wind shear.

Nevertheless, the strong wind shear can increase the strength of the amplitude modulation in wind turbine noise. At long distances in the directions where the blade passes downward, the amplitude-modulated sound occurs when the blades are at the top of the rotor disk, as shown in Fig. 3. Hence, if the vertical wind shear is strong, the effective angle of attack at the top of the rotor disk will increase, as will the sound level of the amplitude-modulated sound in these directions. Furthermore, in the downwind directions, sound rays are bent toward the ground in a strong wind shear.[17] This effect will also raise the level of the amplitude-modulated sound in the downwind directions.

Acknowledgments

References and links

[1]E. Pedersen and K. Persson Waye, "Perception and annoyance due to wind turbine noise—A dose-response relationship," J. Acoust. Soc. Am. **116**, 3460–3470 (2004).

[2]E. Pedersen, F. van den Berg, R. Bakker, and J. Bouma, "Response to noise from modern wind farms in The Netherlands," J. Acoust. Soc. Am. **126**, 634–643 (2009).

[3]G. P. van den Berg, "Effects of the wind profile at night on wind turbine sound," J. Sound Vib. **277**, 955–970 (2004).

[4]S. Oerlemans, P. Sijtsma, and B. Méndez López, "Location and quantification of noise sources on a wind turbine," J. Sound Vib. **299**, 869–883 (2007).

[5]S. Oerlemans and J. G. Schepers, "Prediction of wind turbine noise and validation against experiment," Int. J. Aeroacoust. **8**, 555–584 (2009).

[6]T. F. Brooks, D. S. Pope, and M. A. Marcolini, "Airfoil self-noise and prediction," NASA Reference Publication 1218 (1989).

[7]R. K. Amiet, "Noise due to turbulent flow past a trailing edge," J. Sound Vib. **47**, 387–393 (1976).

[8]R. K. Amiet, "Effect of the incident surface pressure field on noise due to turbulent flow past a trailing edge," J. Sound Vib. **57**, 305–306 (1978).

[9]R. H. Schlinker and R. K. Amiet, "Helicopter rotor trailing edge noise," NASA Contract. Rep. NASA CR **3470**, 14–15 (1981).

[10]J. Casper and F. Farassat, "Broadband trailing edge noise predictions in the time domain," J. Sound Vib. **271**, 159–176 (2004).

[11]Y. Rozenberg, M. Roger, and S. Moreau, "Fan blade trailing-edge noise prediction using RANS simulations," in *Proceedings of Acoustics'08* (2008), pp. 5207–5212.

[12]Y. N. Kim and A. R. George, "Trailing-edge noise from hovering rotors," AIAA J. **20**, 1167–1174 (1982).

[13]T. F. Brooks and T. H. Hodgson, "Trailing edge noise prediction from measured surface pressures," J. Sound Vib. **78**, 69–117 (1981).

[14]K. S. Brentner, "Prediction of helicopter rotor discrete frequency noise—A computer program incorporating realistic blade motions and advanced acoustic formulation," NASA Tech. Memo. **87721**, 6–7 (1986).

[15]http://web.mit.edu/drela/Public/web/xfoil/ (Last viewed October 19, 2012)

[16]ISO 9613-1: *Acoustics—Attenuation of Sound During Propagation Outdoors—Part 1: Calculation of the Absorption of Sound by the Atmosphere* (International Organization for Standardization, Geneva, 1993).

[17]H. H. Hubbard and K. P. Shepherd, "Aeroacoustics of large wind turbines," J. Acoust. Soc. Am. **89**, 2495–2508 (1991).